Front. Earth Sci. 2022, 16(3): 734–743
https://doi.org/10.1007/s11707-021-0920-y

RESEARCH ARTICLE

Examining asymmetric outer-core CAPE in sheared tropical cyclones based on the FNL data set

Yufan DAI[1,2], Qingqing LI (✉)[3,4,5], Lijuan WANG[5], Hong CHEN[6]

1 Nanjing University of Information Science and Technology, Nanjing 210044, China
2 Key Laboratory of South China Sea Meteorological Disaster Prevention and Mitigation of Hainan Province, Haikou 570203, China
3 Pacific Typhoon Research Center, Nanjing University of Information Science and Technology, Nanjing 210044, China
4 State Key Laboratory of Severe Weather, Chinese Academy of Meteorological Sciences, Beijing 100081, China
5 Key Laboratory of Meteorological Disaster (the Ministry of Education), Nanjing University of Information Science and Technology, Nanjing 210044, China
6 Hainan Meteorological Observatory, Haikou 570203, China

Abstract The asymmetric distribution of convective available potential energy (CAPE) in the outer core of sheared tropical cyclones (TCs) is examined using the National Centers for Environmental Prediction Final operational global analysis data. Larger (smaller) CAPE tends to appear in the downshear (upshear) semicircle. This downshear-upshear contrast in CAPE magnitude becomes much more statistically significant in moderate-to-strong shear. The azimuthally asymmetric CAPE is closely associated with the near-surface equivalent potential temperature (θ_e). Larger surface winds occur in the upshear semicircle in strongly sheared TCs, contributing to larger surface latent heat fluxes in those quadrants. More low-level air well fueled by the larger surface latent heat fluxes in the upshear quadrants is cyclonically advected into the downstream quadrants. As a result, larger near-surface θ_e and CAPE are found in the outer core in the downshear quadrants.

Keywords tropical cyclone, outer core, asymmetry, CAPE, reanalysis dataset

1 Introduction

Vertical wind shear (VWS) can induce azimuthally asymmetric convective activity in the outer core (usually outside three times the radius of maximum wind (Wang, 2009)) of tropical cyclones (TCs). For instance, lightning observations have shown the most frequent flash occurrence in the outer core in the downshear-right quadrant (Corbosiero and Molinari, 2002; Stevenson et al., 2014, 2016). Convective cells in the downshear-right quadrant tend to transform into stratiform clouds that are located in the downwind sector of outer rainbands (Hence and Houze, 2008; Houze, 2010; Didlake and Houze, 2013) as the cells move cyclonically. Riemer (2016) found that high-θ_e air and positive vorticity anomalies in the boundary layer on the right of shear play a vital role in developing deep convection. When a TC experiences VWS, its outer rainbands tend to form downshear resulting from convective reinvigoration in the downshear-right quadrant (Li et al., 2017).

Instability is one of the fundamental factors governing the development of deep convection (Schultz et al., 2000). Observations have indicated that VWS can induce azimuthally asymmetric distributions of convective available potential energy (CAPE; Molinari and Vollaro, 2008, 2010; Molinari et al., 2012) within the TC circulation. Larger CAPE values are more predisposed to occur in the downshear quadrant (Molinari and Vollaro, 2008, 2010). The downshear-upshear contrast in the CAPE value becomes more evident when VWS increases (Molinari and Vollaro, 2010). Molinari et al. (2012) argued that the presence of larger CAPE in downshear quadrants results from moister near-surface air, lower mid-level temperature, and larger free-tropospheric relative humidity for entraining CAPE. Li and Dai (2020) further investigated the asymmetric distribution of CAPE in the outer core of sheared TCs through high-resolution numerical experiments. An overarching finding in Li and Dai (2020) is the enhanced downshear-right-downshear-left contrast of

Received February 4, 2021; accepted May 28, 2021

E-mail: liqq@nuist.edu.cn

CAPE in highly sheared TCs. Precipitation-forced downdrafts in outer rainbands cool and dry the downshear-left boundary layer, leading to lower CAPE in that quadrant.

Many studies have examined how reasonably well the location, intensity, structure, and large-scale ambient environments of TCs are represented in reanalysis data sets (Manning and Hart, 2007; Schenkel and Hart, 2012; Hodges et al., 2017), which is valuable for numerical simulations and forecasts of TCs. The characteristics of the distribution of moist instability in reanalysis data sets and its relationship with VWS magnitude are also worth investigating, because they are closely related to numerical modeling of the outer-core convection in TCs. In this study, we will use a reanalysis data set to explore the characteristics of azimuthally asymmetric CAPE in the outer core of sheared TCs. In the next section, the data and methods utilized will be described. The characteristics of the asymmetric distribution of outer-core CAPE will be present in Section 3. We will further examine in Section 4 the features of surface latent heat fluxes, and a summary of the results will be given in the last section.

2 Data and methods

2.1 Data

We will examine the characteristics of CAPE in the outer core of TCs based on the 0.25° × 0.25°, six-hourly National Centers for Environmental Prediction Final (FNL) operational global analysis data. The 0.25° × 0.25° FNL data set is produced from the Global Data Assimilation System and is available since July 2015.

The western North Pacific (WNP) and North Atlantic (NA) TCs from 2016 to 2019 will be investigated here. The general TC information is derived from the International Best Track Archive for Climate Stewardship (IBTrACS) data set (Knapp et al., 2010), containing TC position, intensity, the radius of maximum wind (RMW), and TC translation speed. The best-track data from the National Hurricane Center and the Joint Typhoon Warning Center are used in this study for the North Atlantic and the western North Pacific, respectively. Only the tropical storms and stronger TCs are investigated in this study. Post-tropical cyclones (namely extratropical-transition cases and extratropical cyclones) and post-landfall TCs are also not included. Additionally, TCs with abnormal values of RMW are also excluded. TCs within 500 km of the land are removed from the samples to avert possible land impacts on TCs. As a result, a total of 1800 samples (1029 in the WNP and 771 in the NA) are selected. In the WNP (NA) basin, the proportions of TCs in tropical storms, category-1, category-2, and categories 3–5 are 49.5% (60.1%), 16.6% (19.5%), 12.1% (10.2%), and 21.9% (10.2%) during the period 2016 to 2019, respectively.

2.2 Methods

Environmental factors are directly derived or calculated from the FNL data set, including VWS, sea surface temperatures, and surface wind speed. When we evaluate the CAPE asymmetry in the outer core and compute the VWS, the TC center identified from the FNL data set rather than derived from the IBTrACS is employed. The TC center in the FNL data set is defined as the location of maximum relative vorticity at 850 hPa within a 500 km × 500 km domain centered on the TC position in IBTrACS at corresponding times. Following previous studies (Davis et al., 2008; Galarneau and Davis, 2013; Rios-Berrios and Torn, 2017), to calculate the environmental VWS associated with TCs, the vortex's circulation is first removed from the wind fields of the FNL data set. This is achieved by subtracting the irrotational and nondivergent winds from the entire wind fields within a 500 km radius of the identified TC center. We then calculate wind vectors that mass-weighted layer-averaged between 150 and 300 hPa and between 700 and 925 hPa within a 500 km radius of the identified TC center, respectively. VWS is defined as the vectorial difference in these two wind vectors, as suggested in Velden and Sears (2014).

In this study, the VWS is grouped into three categories in terms of its magnitude. The VWS, with its magnitude below the lower quartile (i.e., 4 $m \cdot s^{-1}$) of all the shear magnitudes, is defined as weak VWS. The VWS, with its magnitude larger than the upper quartile (i.e., 9 $m \cdot s^{-1}$) of all the shear magnitudes, is defined as strong VWS. Correspondingly, the magnitude of moderate VWS is between the lower and upper quartile of all the shear magnitudes.

Surface fluxes, particularly latent heat fluxes, are critical to the change in moist instability. The formula for latent heat fluxes (F_q) that will be used to investigate the contribution of latent heat fluxes to near-surface entropy is as follow:

$$F_q = \rho L_v C_e U[q_s(\mathrm{sst}) - q], \quad (1)$$

where ρ is the density of air (1.2 $kg \cdot m^{-3}$); L_v is the latent heat of vaporization (2.5×10^6 $J \cdot kg^{-1}$); C_e is the exchange coefficients for latent heat transfer (1.2×10^{-3}; Zhang et al., 2008; Bell et al., 2012); U means the wind speed at 10-m height; $q_s(\mathrm{sst})$ is the saturation specific humidity calculated using the sea surface temperature (SST); and q is the near-surface specific humidity from the FNL dataset.

An asymmetry degree (σ_{max}) of CAPE in the outer core is quantified using the asymmetry index defined in Reasor et al. (2013). This index is formulated as:

$$\sigma_{\max}(\mathrm{CAPE}) = \max_{r_1 \leqslant r_i \leqslant r_m} \left\{ \sqrt{\frac{1}{N_i - 1} \sum_{k=1}^{N_i} \left[\mathrm{CAPE}_k(r_i) - \overline{\mathrm{CAPE}}(r_i) \right]^2} \right\}, \quad (2)$$

where r_1 and r_m indicate the inner and outer radii, respectively; N_i is the number of azimuthal grids at a radius of r_i; and the overbar represents the azimuthal mean at a radius of r_i. Here $\sigma_{\max}$ shows the maximum azimuthal standard deviation of CAPE in the selected annular area. The outer core of the TCs that are more intense than tropical storms is defined as an annular region between three times RMW (i.e., $r_1 = 3 \times \mathrm{RMW}$) and eight times RMW (i.e., $r_m = 8 \times \mathrm{RMW}$). In addition, the RMW of TCs in the tropical storm category is much larger than other intensity categories (not shown), and r_m is, thus, set to 5 times the RMW in those TCs to avoid the inclusion of environments.

3 Azimuthally asymmetric distributions of CAPE in the outer core

Figure 1 shows the distribution of the asymmetric indices of outer-core CAPE for different VWS categories. The mean values of the asymmetric indices for weak, moderate, and strong VWS are 397.4, 423.9, and 477.8 $\mathrm{J \cdot kg^{-1}}$ in the WNP basin (Fig. 1(a)), respectively, whereas they are 355.3, 390.1, and 399.1 $\mathrm{J \cdot kg^{-1}}$ in the NA basin (Fig. 1(b)), respectively. The CAPE asymmetric index thus tends to increase with increasing VWS magnitude in both basins. Except for the difference between moderate and strong shear in the NA, there are statistically significant differences between the VWS magnitude categories (at the 95% confidence level based on the permutation test). This result is in line with the findings of idealized numerical experiments in Li and Dai (2020), which documented that the distribution of conditional instability in the outer core becomes more azimuthally asymmetric as VWS increases.

Dropsonde observations showed that larger CAPE is apt to occur in the downshear semicircle of TCs (Molinari and Vollaro, 2008, 2010; Molinari et al., 2012), and high-resolution numerical simulations further indicated that the maximum outer-core CAPE shifts to the downshear-right quadrant in strong VWS (Li and Dai, 2020). The FNL data shows that the mean CAPE in the outer core of sheared TCs in the WNP and NA is greater in the downshear quadrants than in the upshear quadrants (Figs. 2(a), 2(e), and 2(g)), consistent with the results of dropsonde observations. In particular, the differences in the mean CAPE values between the downshear and upshear quadrants are statistically significant (at the 95% confidence level based on the permutation test) for moderate

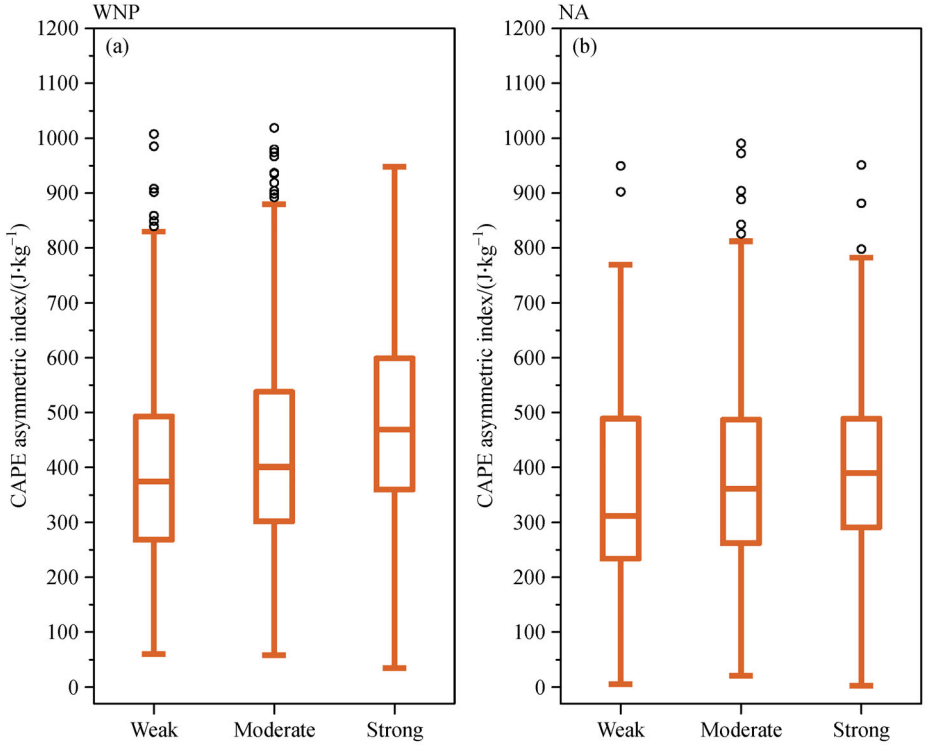

Fig. 1 Boxplots of the asymmetric indices of outer-core CAPE for different VWS categories in the (a) WNP and (b) NA basins (with the lower and upper quartiles as the lower and upper limits of the box, respectively; the median (line in the box); and outliers (black circles)).

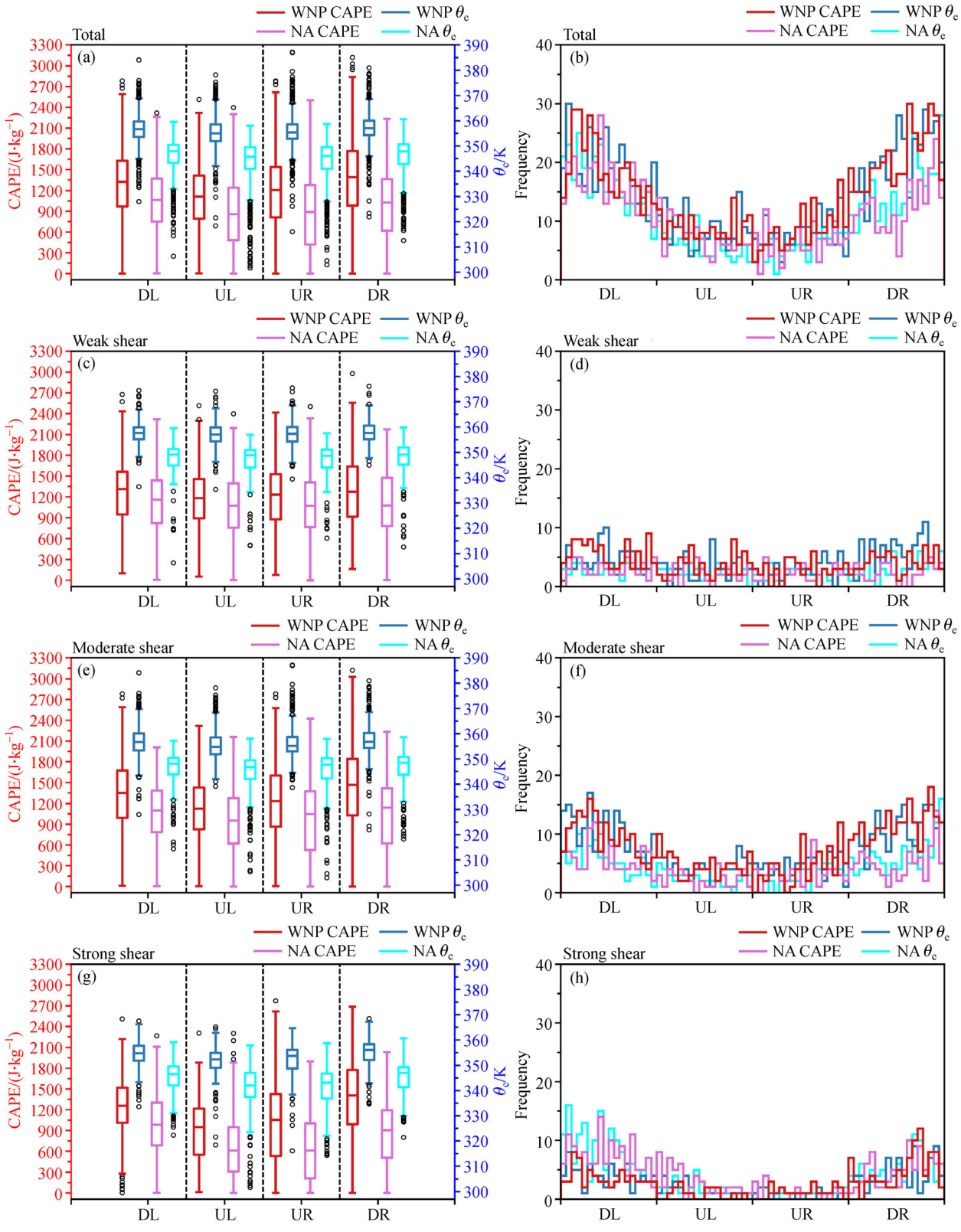

Fig. 2 Boxplots of outer-core CAPE (J·kg^{-1}) and near-surface θ_e (K) averaged in the VWS-relative quadrants for (a) all, (c) weak, (e) moderate, and (g) strong VWS (with the lower and upper quartiles as the lower and upper limits of the box, respectively; the median (line in the box); and outliers (black circles)). Red and lilac boxes indicate the averaged CAPE in the WNP and NA, respectively, and dark blue and cyan boxes indicate the averaged θ_e in the WNP and NA, respectively. The frequency of the azimuthal position of maximum outer-core CAPE and θ_e for all shear, weak, moderate, and strong VWS is shown in (b), (d), (f), and (h), respectively. Red and lilac bars indicate the averaged CAPE in the WNP and NA, respectively, and dark blue and cyan bars indicate the averaged θ_e in the WNP and NA, respectively. "DL," "UL," "UR," and "DR" denote the downshear-left, upshear-left, upshear-right, and downshear-right quadrants, respectively.

and strong VWS (Figs. 2(e) and 2(g)). The difference in mean CAPE between downshear and upshear semicircles is 85.7 (24.9) $J \cdot kg^{-1}$ in the WNP (NA) weak shear cases, while the difference increases to 318.8 (250.2) $J \cdot kg^{-1}$ in the WNP (NA) strong shear cases. This result implies that the asymmetry degree of outer-core conditional instability in the FNL data rises when VWS increases, which is consistent with Li and Dai (2020).

The idealized simulations in Li and Dai (2020) also indicated that the maximum (minimum) CAPE shifts to the downshear-right (downshear-left) outer core when the VWS magnitude increases. The frequency of the azimuthal position of maximum outer-core CAPE is shown in Figs. 2(b), 2(d), 2(f), and 2(h). Compared to the all shear samples (Fig. 2(b)) and weak shear category (Fig. 2(d)), the maximum outer-core CAPE is most frequently observed downshear right for moderate and strong shear categories (Figs. 2(f) and 2(h)), particularly in the WNP. The mean CAPE in the downshear-right quadrant is also larger than that in the downshear-left quadrant in the WNP, with 1415.9 (1337.2) $J \cdot kg^{-1}$ in the downshear-right (downshear-left) quadrant for moderate shear cases and 1344.1 (1240.4 $J \cdot kg^{-1}$) for strong shear cases. However, such a location preference for the maximum CAPE is not evident in the NA (Figs. 2(f) and 2(h)), and the maximum CAPE is even most frequent in the downshear-left outer core for the strong shear category in the NA (Fig. 2(h)). The causes of the quadrant preference difference in the maximum CAPE between the WNP and NA have not yet been clarified, and need further investigations.

4 Contribution of surface latent heat fluxes

The magnitude of surface-based CAPE depends on near-surface entropy and mid-tropospheric temperatures (Williams and Renno, 1993; Ye et al., 1998; Manzato and Morgan, 2003; Molinari et al., 2012). The distribution of near-surface equivalent potential temperature (θ_e) in the outer core is also examined in Fig. 2. As expected, the θ_e vertically averaged between 1000 and 950 hPa is large in the quadrants where CAPE values are large as well (Figs. 2(a), 2(c), 2(e), and 2(g)). The difference in mean θ_e between downshear and upshear semicircles is 0.36 (0.41) K in the WNP (NA) weak shear cases, in contrast to 3.3 (4.7) K in the TCs under strong shear. The averaged θ_e is statistically significantly larger in the downshear quadrant than in the upshear quadrant (at the 95% confidence level based on the permutation test), except for the TCs undergoing weak shear. Additionally, the maximum near-surface θ_e most frequently occurs downshear right for moderate and strong shear categories (Figs. 2(f) and 2(h)), particularly in the WNP. There are no statistically significant differences in mid-tropospheric temperatures among the quadrants (not shown). The above results thus indicate that the azimuthally asymmetric distribution of outer-core CAPE in the FNL data is mainly governed by near-surface θ_e.

Surface latent heat fluxes are proportional to surface wind velocity and air-sea humidity deficits in terms of Eq. (1). The characteristics of surface wind velocity and air-sea humidity deficits in the outer core will, thus, be investigated here to examine their contributions to the latent heat fluxes and near-surface entropy. Figure 3 shows the distribution of air-sea humidity disequilibrium ($\Delta Q = q_s(\mathrm{sst}) - q$) in the outer core for different shear categories in the WNP and NA basins, and the characteristics of surface wind speeds relative to TC translation in these two basins are presented in Fig. 4.

The quadrant-averaged value of ΔQ ranges mainly from 1 to 8 $g \cdot kg^{-1}$, comparable to the result in Nguyen et al. (2019) that showed ΔQ values between 3 and 7 $g \cdot kg^{-1}$. Note that there is negative ΔQ which is generally associated with the TCs at relatively high latitudes (near or larger than 40°N) and occurring in nonactive TC seasons (namely before March or after October). Although the mean ΔQ is larger in the WNP than in the NA (Figs. 3(a), 3(c), 3(e), and 3(g)), there is no statistically significant difference in ΔQ values between quadrants and shear categories. Moreover, the frequency of the maximum ΔQ is nearly similar (Figs. 3(b), 3(d), and 3(f)), except for the TCs under strong shear in the NA basin (Fig. 3(h)). Larger ΔQ is disposed to arise on the right of strong shear in the NA. The strong-shear cases in the NA basin mainly experience northwesternly VWS. Relatively smaller ΔQ on the left of strong shear is probably due to cold advection from the mid-latitudes. The details pertaining to the characteristics of ΔQ in strong VWS in the NA need further investigations.

Maximum surface winds prefer to occur in the upshear semicircle in the WNP and NA basins (Figs. 4(b), 4(d), 4(f), and 4(h)). In the WNP and NA, the mean value of surface wind velocity is smaller in the downshear quadrants than in the upshear quadrants (Fig. 4(a)). In particular, such an asymmetry is more evident when the TCs undergo moderate to strong shear (Figs. 4(e) and 4(g)) than weak shear (Fig. 4(c)). This result seems to be different from inner-core wind velocity. Zhang et al. (2013) employed dropsonde data to examine the asymmetric boundary layer structure in sheared TCs. It showed that near-surface tangential winds within the inner core are larger on the left of VWS than on the right of VWS, approximately 90° upwind of the larger wind in the outer core indicated here. Chen et al. (2021) showed azimuthal asymmetries of helicity in the TC boundary layer based on dropsonde data. They also inferred that asymmetric distributions of surface wind in sheared TCs lead to the azimuthal asymmetries of helicity.

Given the azimuthally asymmetric distribution of surface wind velocity in the outer core, surface latent

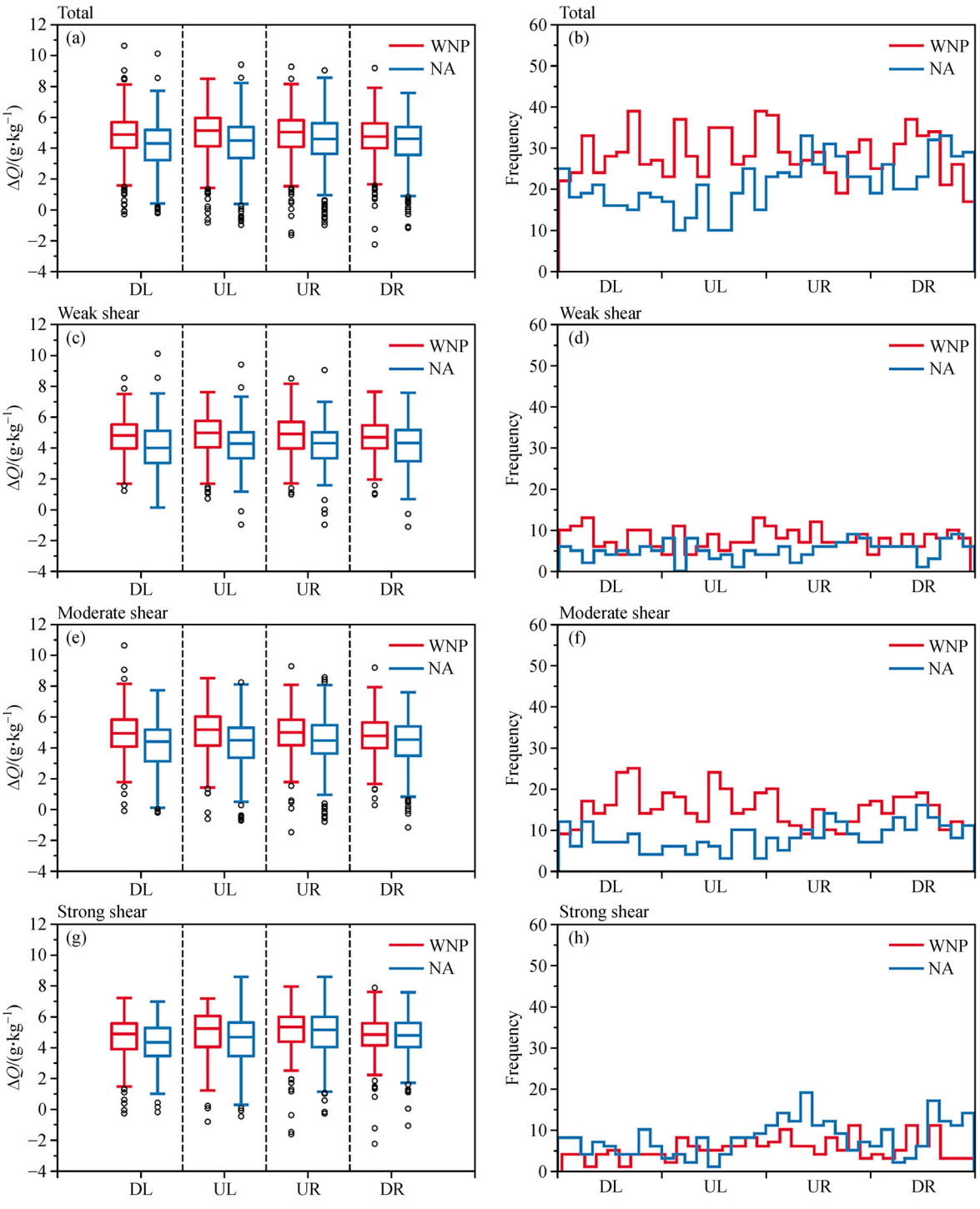

Fig. 3 Boxplots of air-sea humidity deficits ($\times 10^{-3}$ kg·kg^{-1}) in the outer core, averaged in the VWS-relative quadrants for (a) all, (c) weak, (e) moderate, and (g) strong VWS (with the lower and upper quartiles as the lower and upper limits of the box, respectively; the median (line in the box); and outliers (black circles)). Red and dark blue boxes indicate the averaged air-sea humidity deficits in the WNP and NA, respectively. The frequency of the azimuthal position of maximum outer-core air-sea humidity deficits for all shear, weak, moderate, and strong VWS is shown in (b), (d), (f), and (h), respectively. Red and dark blue bars indicate the averaged air-sea humidity deficits in the WNP and NA, respectively. "DL", "UL", "UR", and "DR" denote the downshear-left, upshear-left, upshear-right, and downshear-right quadrants, respectively.

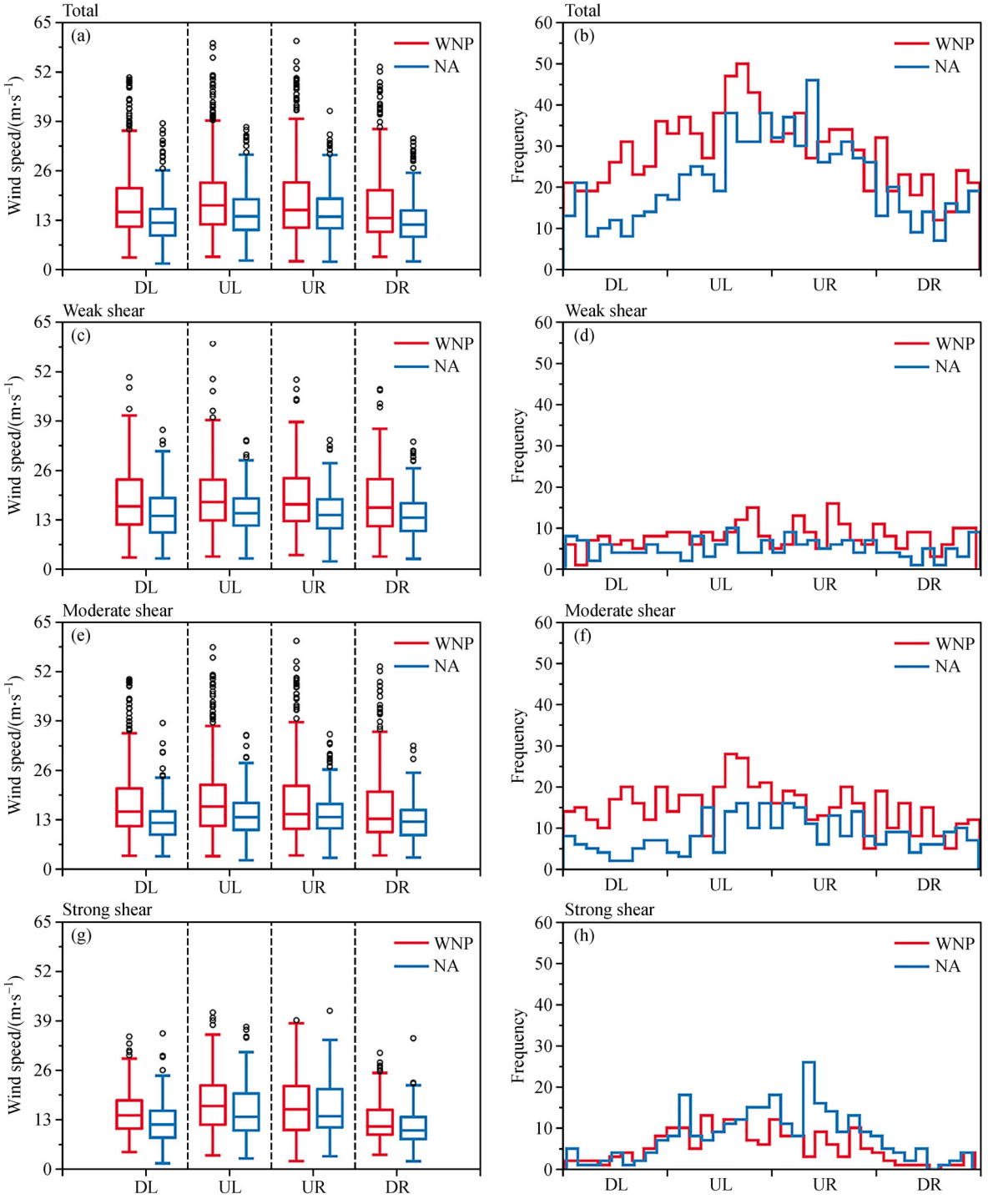

Fig. 4 As in Fig. 3, but for surface wind velocity.

heat fluxes are asymmetrically distributed for different shear categories. Figure 5 shows that quadrant-averaged values of latent heat fluxes in the outer core are mainly around 200–300 $W \cdot m^{-2}$. Note that negative latent heat fluxes are because of negative ΔQ in the TCs at high latitudes. The distribution of quadrant-averaged latent heat fluxes is similar to that of surface wind fields, with larger latent heat fluxes predominantly in the upshear quadrants (Fig. 5(a)), particularly for moderate and strong VWS (Figs. 5(e) and 5(g)). Quadrant-averaged latent heat fluxes are minimized in the downshear-right quadrant (Figs. 5(a), 5(e), and 5(g)) except for the weak shear category (Fig. 5(c)). Also, surface latent heat fluxes peak more frequently in the upshear quadrants (Figs. 5(b), 5(f),

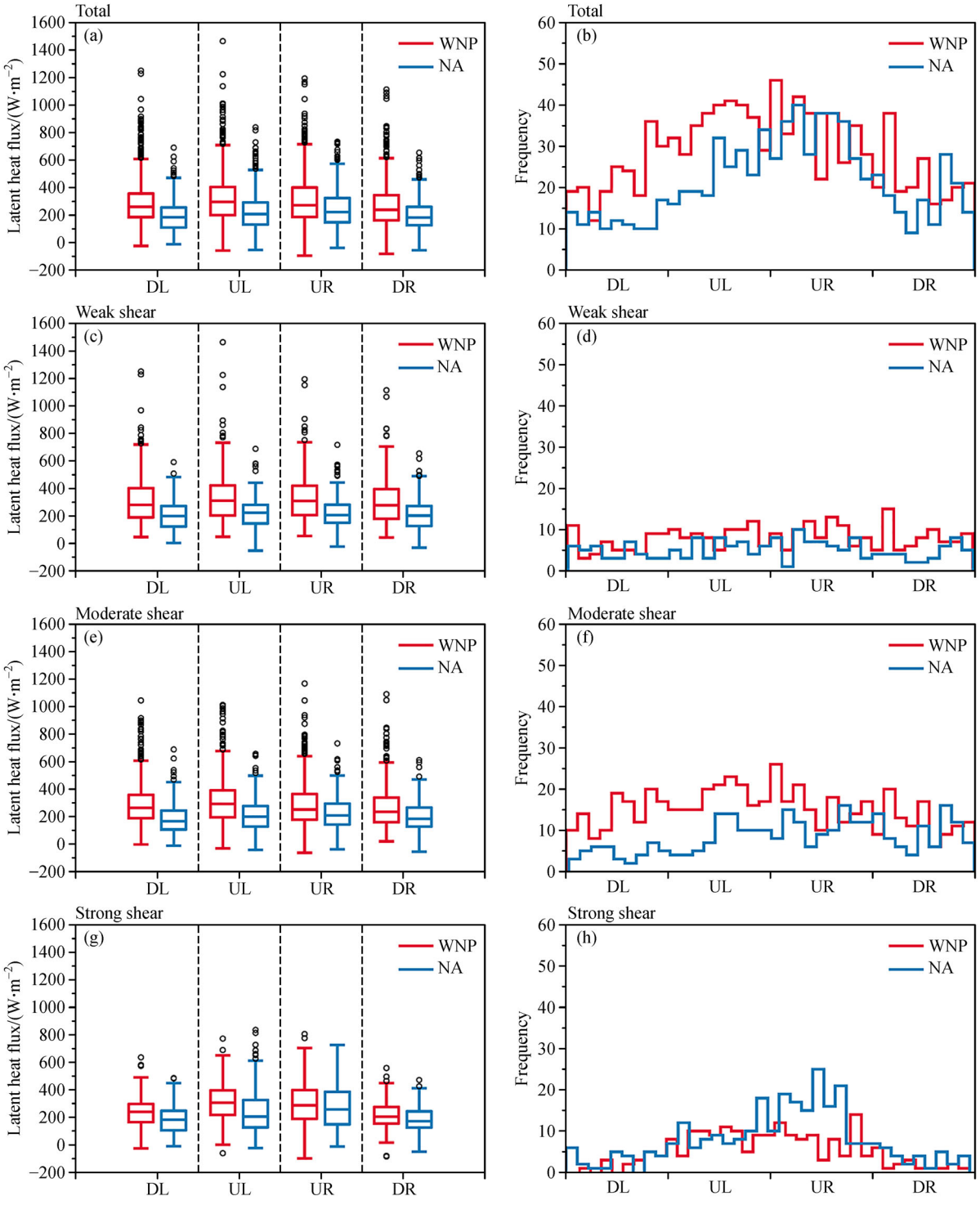

Fig. 5 As in Fig. 3, but for surface latent heat fluxes.

and 5(h)). The above results indicate that surface wind velocity is the more dominant contributor to the azimuthally asymmetric distribution of surface latent heat fluxes in sheared TCs in the FNL reanalysis data set.

Figure 2 shows that larger near-surface θ_e and CAPE mainly occurs in the downshear outer core for moderate-to-strong shear, while the surface latent heat fluxes in the outer core are larger in the upshear quadrants. There appears to be a quadrant imbalance between the larger near-surface entropy and surface latent heat fluxes. Figure 4 indicates that surface winds are faster in the upshear quadrants than in the downshear quadrants. More

low-level air that is more significantly fueled by the larger surface latent heat fluxes in the upshear quadrants is cyclonically advected into the downstream quadrants. As a result, larger near-surface θ_e and CAPE, thus, exist in the downshear quadrants.

5 Summary

In the current study, we examined the asymmetric distribution of CAPE in the outer core of TCs based on the FNL reanalysis. The results indicate that the distribution of outer-core conditional instability becomes more azimuthally asymmetric with increasing environmental VWS, which is akin to the findings of idealized numerical experiments in previous studies. Larger (lower) CAPE arises in the downshear (upshear) quadrants. This downshear-upshear contrast in CAPE is much more statistically significant in moderate-to-strong shear.

Asymmetric surface latent heat fluxes significantly contribute to the existence of azimuthal asymmetries of θ_e and CAPE in the outer core of sheared TCs. Larger latent heat fluxes predominantly occur in the upshear quadrants, particularly for moderate and strong VWS, where the surface winds are larger as well. The above results indicate that surface wind velocity is the more dominant contributor to the azimuthally asymmetric distribution of surface latent heat fluxes in sheared TCs in the FNL reanalysis data set. Although larger latent heat fluxes appear in the upshear quadrants in the outer core, more low-level air with enhanced entropy is advected from the upshear quadrants into the downstream quadrants. Resultantly, larger θ_e near the surface and, thus, CAPE exhibit in the downshear quadrants.

Previous high-resolution modeling studies (Li and Dai, 2020) have indicated that the maximum CAPE and near-surface θ_e are preferentially located downshear right in the outer core of highly sheared TCs. However, the minimum CAPE and near-surface θ_e occur downshear left due to the most marked evaporative cooling within outer rainbands. In the FNL reanalysis data set, the lowest CAPE and near-surface θ_e are not found in the downshear-left quadrant. This indicates that the FNL reanalysis data set likely fails to capture the precipitation structures and associated evaporative cooling in outer rainbands. Therefore, data assimilation within the outer core of TCs, particularly within outer rainbands, is important when the FNL reanalysis data set is used as the initial conditions in TC simulations.

Acknowledgements This work was jointly supported by the National Key Research and Development Program of China (No. 2017YFC1501601), the National Natural Science Foundation of China (Grant Nos. 41475058, 41730961, 41675044, 41730960, and 41875054), and the Key Laboratory of South China Sea Meteorological Disaster Prevention and Mitigation of Hainan Province Foundation (No. SCSF202003).

References

Bell M M, Montgomery M T, Emanuel K A (2012). Air-sea enthalpy and momentum exchange at major hurricane wind speeds observed during CBLAST. J Atmos Sci, 69(11): 3197–3222

Chen N, Tang J, Zhang A J, Ma L M, Yu H (2021). On the distribution of helicity in the Tropical Cyclone boundary layer from dropsonde composites. Atmos Res, 249: 105298

Corbosiero K L, Molinari J (2002). The effects of vertical wind shear on the distribution of convection in Tropical Cyclones. Mon Weather Rev, 130(8): 2110–2123

Davis C, Snyder C, Didlake A C Jr (2008). A vortex-based perspective of eastern Pacific Tropical Cyclone formation. Mon Weather Rev, 136(7): 2461–2477

Didlake A C, Houze R A (2013). Dynamics of the stratiform sector of a Tropical Cyclone rainband. J Atmos Sci, 70(7): 1891–1911

Galarneau T J Jr, Davis C A (2013). Diagnosing forecast errors in Tropical Cyclone motion. Mon Weather Rev, 141(2): 405–430

Hence D A, Houze R A (2008). Kinematic structure of convective-scale elements in the rainbands of Hurricanes Katrina and Rita (2005). J Geophys Res, 113(D15)

Hodges K, Cobb A, Vidale P L (2017). How well are tropical cyclones represented in reanalysis datasets? J Clim, 30(14): 5243–5264

Houze R A, (2010). Clouds in Tropical Cyclones. Mon Weather Rev, 138(2): 293–344

Knapp K R, Kruk M C, Levinson D H, Diamond H J, Neumann C J (2010). The international best track archive for climate stewardship (IBTrACS). Bull Am Meteorol Soc, 91(3): 363–376

Li Q, Dai Y (2020). Revisiting azimuthally asymmetric moist instability in the outer core of sheared Tropical Cyclones. Mon Weather Rev, 148(3): 1297–1319

Li Q, Wang Y, Duan Y (2017). A numerical study of outer rainband formation in a sheared tropical cyclone. J Atmos Sci, 74(1): 203–227

Manning D M, Hart R E (2007). Evolution of North Atlantic ERA40 Tropical Cyclone representation. Geophys Res Lett, 34(5): 3–6

Manzato A, Morgan G Jr (2003). Evaluating the sounding instability with the Lifted Parcel Theory. Atmos Res, 67–68: 455–473

Molinari J, Romps D M, Vollaro D, Nguyen L (2012). CAPE in Tropical Cyclones. J Atmos Sci, 69(8): 2452–2463

Molinari J, Vollaro D (2008). Extreme helicity and intense convective towers in Hurricane Bonnie. Mon Weather Rev, 136(11): 4355–4372

Molinari J, Vollaro D (2010). Distribution of helicity, CAPE, and shear in Tropical Cyclones. J Atmos Sci, 67(1): 274–284

Nguyen L T, Rogers R, Zawislak J, Zhang J A (2019). Assessing the influence of convective downdrafts and surface enthalpy fluxes on Tropical Cyclone intensity change in moderate vertical wind shear. Mon Weather Rev, 147(10): 3519–3534

Reasor P D, Rogers R, Lorsolo S (2013). Environmental flow impacts on Tropical Cyclone structure diagnosed from airborne doppler radar composites. Mon Weather Rev, 141(9): 2949–2969

Riemer M (2016). Meso-β-scale environment for the stationary band complex of vertically sheared tropical cyclones. Q J R Meteorol Soc, 142(699): 2442–2451

Rios-Berrios R, Torn R D (2017). Climatological analysis of Tropical Cyclone intensity changes under moderate vertical wind shear. Mon

Weather Rev, 145(5): 1717–1738

Schenkel B A, Hart R E (2012). An examination of tropical cyclone position, intensity, and intensity life cycle within atmospheric reanalysis datasets. J Clim, 25(10): 3453–3475

Schultz D M, Schumacher P N, Doswell C A III (2000). The intricacies of instabilities. Mon Weather Rev, 128(12): 4143–4148

Stevenson S N, Corbosiero K L, Abarca S F (2016). Lightning in eastern North Pacific tropical cyclones: a comparison to the North Atlantic. Mon Weather Rev, 144(1): 225–239

Stevenson S N, Corbosiero K L, Molinari J (2014). The convective evolution and rapid intensification of Hurricane Earl (2010). Mon Weather Rev, 142(11): 4364–4380

Velden C S, Sears J (2014). Computing deep-tropospheric vertical wind shear analyses for tropical cyclone applications: does the methodology matter? Weather Forecast, 29(5): 1169–1180

Wang Y (2009). How do outer spiral rainbands affect tropical cyclone structure and intensity? J Atmos Sci, 66(5): 1250–1273

Williams E, Renno N (1993). An analysis of the conditional instability of the tropical atmosphere. Mon Weather Rev, 121(1): 21–36

Ye B, Del Genio A D, Lo K K W (1998). CAPE variations in the current climate and in a climate change. J Clim, 11(8): 1997–2015

Zhang J A, Black P G, French J R, Drennan W M (2008). First direct measurements of enthalpy flux in the hurricane boundary layer: the CBLAST results. Geophys Res Lett, 35(14): L14813

Zhang J A, Rogers R F, Reasor P D, Uhlhorn E W, Marks F D Jr (2013). Asymmetric hurricane boundary layer structure from dropsonde composites in relation to the environmental vertical wind shear. Mon Weather Rev, 141(11): 3968–3984